Optimization framework for evaluating urban thermal systems potential

B Nérot, N Lamaison, Mohamed Tahar Mabrouk, R Bavière, B Lacarrière

Optimization framework for evaluating urban thermal systems potential

B. Nérot[a, b], N. Lamaison[a], M.T. Mabrouk[b], R. Bavière[c], B. Lacarrière[b*]

[a]*Univ Grenoble Alpes, CEA, LITEN, Campus INES, 73375 Le Bourget du Lac, France*
[b]*IMT Atlantique, Department of Energy Systems and Environment, GEPEA, F-44307, Nantes, France*
[c]*Univ Grenoble Alpes, CEA, LITEN, DTCH, 38000 Grenoble, France*
*corresponding author, *bruno.lacarriere@imt-atlantique.fr*

Abstract

The increase in space cooling demand worldwide calls more than ever for efficient ways to meet buildings combined hot and cold demands.

Building scale technologies present interesting advantages such as modularity but also numerous drawbacks such as architectural issues, urban heat island effect, low efficiency and stress on the electrical network. Yet, a literature gap exists regarding the optimal equilibrium between local and centralized thermal equipment.

This paper presents a framework to evaluate the performances of urban thermal architectures. It relies on an existing building typology database to derive hourly profiles of space heating, space cooling and domestic hot water demands. An object-oriented energy hub implementation eases the gathering of production, storage and distribution components. Optimal components are finally selected through a MILP-based optimization.

The framework application shows its abilities to sort pre identified thermal architectures by performance level. For the addressed case studies, 4th generation district heating (4GDH) performs the best regarding CO_2 emissions and exergy destruction, while 2GDH is often cost-effective. In the selected configurations, 5thgeneration district heating and cooling (5GHDC) performs hardly better than individual solutions.

The use of different components depending on the techno-economic context indicates the need to challenge many solutions, which is possible using the framework.

Keywords: framework; heating; cooling; architecture; comparison; mixed-integer linear programming

1 Introduction

Nomenclature

Variables	
$a_{b,SH}$	Helper parameter for gain utilization factor (-)
A	Floor area (SH, SC, DHW) (m^2)
A^{grd}	Ground area (m^2)
A^{sizing}_{prod}	Sizing area of a solar thermal component (m^2)
c_p	Specific heat capacity of water ($J/(kg.K)$)
D	Diameter (m)
e	Plot ratio (-)
f_Q	HP COP parameter - compressor heat loss ratio (-)
E	Non thermal energy (gas, biomass or electricity) (J)
F	Energy transfer between a hub and its environment (J)
H	Overall heat transfer coefficient (W/K)
L	Length (m)
n	Technological lifetime (years)
p	Proportion (%)
Q	Thermal energy (J)
r	Actualization rate (%)
t	Time
t_{reg}, pc^{min}_{peak} and pc^{max}_{peak}	Parameters for variable time step approach
TSV_{hourly}, TSV_{va}	One-hour and variable time step vectors
T	Temperature
T_0	Exergy reference temperature
U	Specific heat loss per routed meter of network trench ($W/(K.m)$)
V	Volume (L)
w	Effective width (m)
ϵ	Storage losses ($\%/h$)
$\gamma_{b,SH}$	Heat balance ratio for the heating mode (-)
$\eta_{is,c}$	HP COP parameter – compression efficiency (-)
η_{prod}	Efficiency (%)
$\eta_{b,SH}$	Gain utilization factor for heating (-)
ϕ	Heat gain (J)
Subscripts	
b	Building
c	Component of type production, storage or energyIO
d	Thermal demand (SH: space heating, DHW: domestic hot water, SC: space cooling)
$energyIO$	EnergyIO component
h	Energy hub
$loss$	Thermal losses
net	Network component
P	Set of production components
$prod$	Production component
$source$	Thermal vector used by a component to take energy from
S	Set of storage components
$stor$	Storage component
v	Energy vector
$air, int, sol, soil$	Ambient air, Internal, Solar, Soil
Superscripts	
A	Relative to an area
$cold, hot$	Cold and warm thermal vectors associated with a component
$drive$	Thermal vector that powers a heat-driven absorption chiller, gives energy to the component
sys	Relative to the energy system
$sink$	Thermal vector used by a component to give energy to
$sizing$	Relative to the sizing of the component
Acronyms	
$CAPEX$	Investment cost ($€/W, €/\mathrm{m}^3 or\ €/m$)
CC	Carbon content
CHP	Combined Heat and Power
CPP	Central Production Plant
CR	Centralization rate
DC	District cooling
DH	District heating
DHW	Domestic hot water
DRC	Dry cooler
EX	Exergy
HEx	Heat exchanger
HP	Heat pump
$LCOE$	Levelized cost of energy
LP	Linear programming
LR/HR	Low/High thermal retrofitting of buildings
$MILP$	Mixed-integer linear programming
$OPEX_F$	Fixed operation/maintenance cost ($\%CAPEX/yr$)
$OPEX_V$	Variable operation/maintenance cost ($€/MWh$)
PEF	Primary Energy Factor
IEH	Industrial Excess Heat
SC	Space cooling
SFH/MFH	Single family house/Multi family house
SH	Space heating
STh	Solar thermal
Operators	
max	Maximum
min	Minimum
$\dot{}$	Temporal derivative
$\bar{}$	Upper bound of a MILP variable
Δ	Difference
$(a_1, b_1) \xrightarrow{x} (a_2, b_2)$	Continuous function f of the x variable: $\forall x \in \mathbb{R}, f(x) = \begin{cases} b_1 \ if\ x \le a_1 \\ b_2 \ if\ x \ge a_2 \\ b_1 + \frac{x-a_1}{a_2-a_1} \times (b_2 - b_1) else \end{cases}$

1.1 Context

Global warming will cause an increase in the cooling needs of buildings in the upcoming years. Especially, this is expected to reach 240 TWh in Europe by 2050 [1], i.e. a multiplication by 1.6 compared to 2016. Moreover, only low-carbon energy vectors must be considered to satisfy this demand, in compliance with the 2015 Paris Agreements [2]. Space heating (SH) and domestic hot water (DHW) demands are expected to decline but are framed by the same decarbonization context as space cooling (SC).

Most of these combined demands exist in urban areas [1] in residential and tertiary buildings. The properties and occupant behaviors of these buildings differ. Consequently, the equipment used to meet these demands are case dependent. Some are individual systems installed within the buildings (e.g.: heat pumps and chillers, boilers, electric heating), others depend on thermal networks to enhance vector synergies and renewables integration [3].

So far, different kinds of tools have been used for the design stage of thermal energy systems. Those tools account for environmental and energy targets, in addition to cost efficiency. The computational complexity of optimization methods grows with the modelling level of details [4]. Thus, there is a need for a framework allowing the comparison of several urban energy systems in their ability to satisfy heat and cold demands.

1.2 State-Of-the-Art

Casisi et al. [5] consider the sizing and operation of a 9 tertiary buildings energy system using the Mixed Integer Linear Programming (MILP) formalism. Life cycle cost is minimized while CO_2 emissions are constrained using an epsilon formulation type of multi-objective optimization. Four kinds of demand are considered, SH, DHW, SC and electricity. Individual or centralized equipment are used to fulfill these demands and whether two buildings are connected together is up to the optimizer. A typical day approach reduces the large computational complexity of the problem. Lazzeroni et al. [6]solve a similar energy system in the Italian case, with a focus on the economic part. An increase in the cost of heat bought from a third-party provider leads to question the value of a new district heating (DH) system. Their work differs from Casisi et al. [5] as a spatial aggregation of demands is performed so that thermal energy generation occurs only at a central unit. Moreover, only the operational part is computed by the solver since the system design is fixed in a few predefined scenarios. The synergies between heat and cold production are also addressed by Fahlén et al. [7]. They use a least-marginal production cost approach to quantify the cost and CO_2 emissions savings when compression chillers are replaced by DH-driven absorption chillers in a central production plant. Chardon et al. [8] analyze the installation of the same kinds of chillers but in a decentralized fashion, i.e. in DH substations. Their study, which covers different operating modes and temperatures, highlights the potential regarding the distribution network as a whole. Bartolozzi et al. [9] study the polygeneration of heat and cold disregarding the economic indicators. They assess the environmental impact of a District Heating and Cooling (DHC) system from the assembly to its end-of-life stages. Though this work does not present a design metho dology of thermal energy systems, it emphasizes how thermal architectures that perform similarly from an energetic point of view affect the environment differently. The studied DH network is located in Italy and consists in 250 dwellings energy systems where all SH, SC and DHW demands coexist.

Several other works consider only the heating demand. This is the case of Kouhia et al. [10] who establish an almost linear MILP implementation of a DH central production unit. The novelty of their work is the optimization of the system in a multi-objective approach (using the method from Lee et al. [11]). In addition to traditional cost, CO_2 operating emissions, and local exergy efficiency, the primary energy factor (PEF) of fossil and non-fossil fuels characterizes the energy performance of the system. Differently from Kouhia et al. [10], Morvaj et al. [12] explore shared decentralized heat generation with no central unit. Their model is similar to Casisi et al. [5] but of lower complexity since the number of variables and constraints is around ten times smaller because of i) a smaller number of typical days and ii) constant efficiencies of heat production equipment.

Finally, some studies set the detailed operational part aside in the evaluation of urban thermal energy systems. Dahl et al. [13] consider a DH system with parametric scenarios regarding the impact of wind power integration on electricity cost and thus cogeneration units profitability. They rely on a low-complexity LP model. For older DH systems, Dzenajaviciene et al. [14] detail the economic contexts that make the retrofitting of 2nd generation networks cheaper than the use of individual solutions. Likewise, Jangsten et al. [15] deal with the existing DC network of Gothenburg. The authors evaluate how a reduction of building system temperatures (demand side) would benefit to the river passive cooling (production side), thus increasing the performance of the network. Gustafsson et al. [16] also challenge centralized solutions. They run several Monte-Carlo simulations in an attempt to reveal the techno-economic scenarios that benefit to individual compression heat pumps, compared to a 3rd generation DH network, for low-density housing areas. Whereas Dahl et al.[13] and

Gustafsson et al. [16] quantify the dependency in production, storage and energy costs of the systems design, Best et al. [17] focus on the network layout and pipe sizing, using a MILP-based model. The novelty of their approach is the minimization of the life cycle costs, including those related to pressure drop and heat losses.

Overall, some of the models reviewed in the state-of-the-art lack the aspects of thermal production and storage at the building level [6,7,10,13]. Others do not consider the existence of a cooling demand [9,12,14,16]. In [5], the optimization of the network topology according to building locations is a strong feature but cannot be realistically extrapolated to a city-wide energy system. From a broader point of view, the advanced operational constraints presented in MILP models [5,6,12] make the system design more realistic but at the cost of long solving time and few modelling flexibility when it comes to rearranging production and storage components[4].

1.3 Contribution and organization of the article

This article presents a framework to evaluate the performances of centralized and decentralized urban thermal architectures. A common modelling approach is taken for different architectures, giving the framework a versatility feature. Moreover, and contrary to existing models, this framework enables the study of city-wide energy systems. This is achieved by applying the energy hub concept [18]on a limited number of nodes, thanks to thermal demand aggregation at the city scale (part 2.2). This demand is defined using a semi-statistic prediction model for residential buildings (part 2.1) not only for SH but also regarding DHW and SC demands. Part 3 presents a comparison of four of the most widespread thermal architectures with respect to Levelized Cost of Energy (LCOE), CO_2 emissions and exergy efficiency. On the one hand, part 3.1 sets a common techno-economic context through properties of production and storage components adapted to this case study. On the other hand, part 3.2 defines parametric scenarios regarding thermal demand and properties of energy vectors. Results are presented in part 4 while part 5 expands on the benefits and limitations of the framework.

2 Thermal architectures evaluation framework

2.1 Thermal demands of residential buildings

This part describes the model developed to calculate representative hourly SH, SC and DHW demands.

2.1.1 Space heating and cooling demands

The Tabula-Episcope project [19]has two main goals:

- To collect the construction properties of existing residential European buildings.
  The resulting database classifies buildings accordingly to their country, construction period, size and level of thermal retrofitting.
- To use these properties to assess their annual SH and DHW energy consumption.
  SH demand per unit area $(kWh/(m^2.yr))$covers solar and transmission heat gains using annual weather data.

The following two points were out of the scope of Tabula project: i) SC demand of buildings and ii) evaluation of thermal demand at a finer temporal scale than yearly average. A new model is introduced and referred to as “adapted model”. It is based on an hourly time step, covers SC demand and considers the same energy contributions as the Tabula model.
Equation (1) presents the SH demand $(kW/m^2)$for building b at time$t$.

$$\dot{Q}^{A}_{b,SH}(t) = max\left(H^{A}_{b}\left(T_{SH} - T_{air}(t)\right) - \eta_{b,SH}\left(\dot{Q}^{A}_{int} + \dot{\phi}^{A}_{sol,b}(t)\right), 0\right) \text{ with } S = \begin{cases} 1\ if\ d = SH \\ -1\ if\ d = SC \end{cases} \quad (1)$$

With $\eta_{b,SH}$ the gain utilization factor for heating defined by Equations (*2*) and (*3*). Parameter $a_{b,SH}$ depends on the time constant of the building.

$$\eta_{b,SH} = \frac{1 - {\gamma_{b,SH}}^{a_{b,SH}}}{1 - {\gamma_{b,SH}}^{a_{b,SH}+1}} \quad (2)$$

$$\gamma_{b,SH} = \frac{\sum_t \left(\dot{\phi}^A_{sol,b}(t) + \dot{Q}^A_{int}\right)}{\sum_t H^A_b \left(T_{SH} - T_{air}(t)\right)} \quad (3)$$

The SC demand is defined by Equation (*4*).

$$\dot{Q}^A_{b,SC}(t) = max\left(\left(\dot{Q}^A_{int} + \dot{\phi}^A_{sol,b}(t)\right) - H^A_b\left(T_{SC} - T_{air}(t)\right), 0\right) \quad (4)$$

T_{SH} and T_{SC} are the indoor set point temperatures. Solar gain $\dot{\phi}^A_{sol,b}(t)$ is calculated considering the same reduction factors as in Tabula, yet using an instantaneous solar gain vector instead of annual irradiation values. This vector originates from an orthogonal projection of the solar position vector on the normal vector of each window area. Internal gains follow the Tabula value, i.e. $\dot{Q}^A_{int} = 3W/m^2$. No SC/SH exists during the heating season/cooling season.

The annual SH demand obtained using adapted and Tabula models are compared with each other on a subset of Tabula buildings. The details presented in Appendix 6.1 validate the adapted model.

Though the SH and SC demand model is particularly suitable for European countries due to properties of building being tabulated, it could be extended to any climate dry enough so that latent cooling load can be neglected.

2.1.2 DHW demand

The hourly draw-off profile $\dot{Q}^A_{DHW}(t)$ is deduced from a DHWCalc [20] profile generated for a thousand living units, i.e. a number large enough to cover most of the simultaneity at city scale [21] (see part 2.2.2). Additionally, DHW circulation losses lead to a constant demand that accounts for 40% of the annual DHW demand, which is $Q^A_{DHW} = 20\ kWh/(m^2.yr)$.

The peak DHW demand is a function of the number of apartments of the building. It is derived from a DHWCalc profile using a 15 min time step. Table *1* presents the corresponding hypothesis. That model typically yields $\dot{Q}^{sizing}_{b,DHW} = 41\ kW$ and $\dot{Q}^{sizing}_{b,DHW} = 108\ kW$ for a 1-apartment and 20-apartments building respectively, where apartments are 60 m² each.

Table 1: Temperatures for DHW demand calculation (°C)

	Operation	Sizing
Cold water	16	11
Warmed water	40	60

2.2 Optimization model

This part presents the modelling choices that adapt a city-wide thermal energy system to a MILP problem with few integer variables.

2.2.1 Energy hub definition

Geidl et al. define energy hubs as centralized units that can handle transformation, conversion and storage of various forms of energy and exchange them with each other[18], or with the surrounding environment. Historically, these operations performed on energy vectors have often been modelled using coupling matrices (e.g. [22,23]) allowing high computational efficiencies but small modelling flexibility.

The energy system considered in this paper consists in residential urban buildings. The satisfaction of their thermal demands is achieved using either local components (all energy flows are related to the building) or centralized components (some energy is exchanged with a central entity).The energy hub concept is particularly suited for this approach, as shown in Figure *1*.

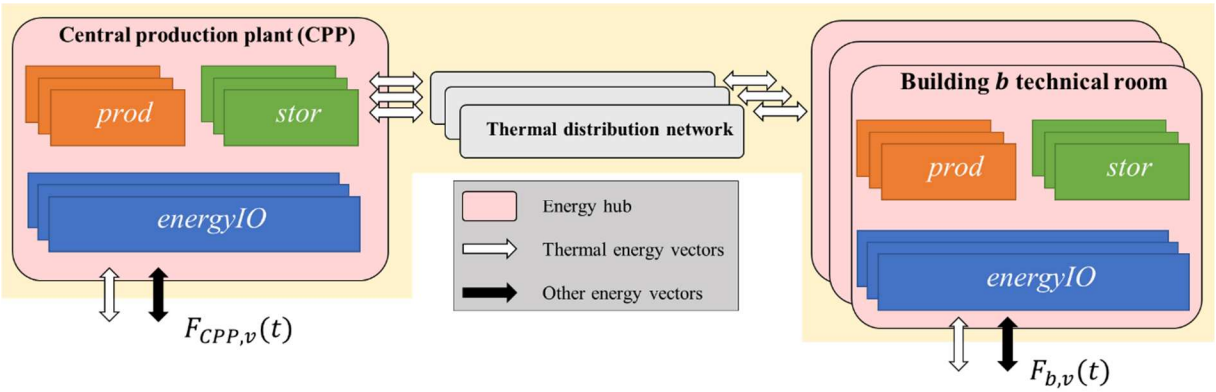

Figure 1: Overview of the energy system.
Buildings rely either on the network thermal energy or on local production to meet their thermal demands.

A typical study is made of the following steps:

1. Problem parameterisation:
   a. Definition of energy vectors v. Thermal energy vectors are either infinite (one temperature and no c_p, e.g. ambient air) or finite (cold and warm temperatures and c_p is defined, e.g. flow being cooled down).
   b. Parameterization of production, storage and energyIO components and declaration of potential connections between energy hubs h using distribution networks.
   c. Selection of an objective function.
2. Problem declaration:
   a. Powers associated with energy vectors are exchanged between components using operation-related decision variables. Design-related variables (e.g. max power) are bound to these variables.
   b. Components contribute to the objective function.
3. Problem resolution: using a MILP solver.

Points 1 and 2 are implemented in Python 3 following an object-oriented paradigm that fits well with the energy hub concept. Points 2 and 3 rely on the Docplex API [24] and Cplex solver (version 20.1).

2.2.2 Spatial approach

A set of thermal demands is built at the city scale by approximating every real building to one of the Tabula database. The plot ratio describes the ratio of floor area subjected to thermal demands to the ground area of the district. The methodology used here is an adaptation of the work of Persson et al. [25].

Equations(5), (6) and (7) give respectively the total thermal area (A^{sys}), the thermal area of buildings assimilated to type $b(A_b^{sys})$ and the weighted plot ratio (e).The city ground area (A^{grd}), plot ratio (e_b) and proportion (p_b) of building b are three parameters.

$$A^{sys} = eA^{grd} = \sum_b A_b^{sys} \quad (5)$$

$$A_b^{sys} = p_b A^{sys} \quad (6)$$

$$e = \frac{1}{\sum_b \frac{p_b}{e_b}} \quad (7)$$

The thermal area of every building of type b in the system $\left(A_b^{sys}\right)$ defines the instantaneous SH, SC and DHW demands at the city scale for this particular type of building (Equation (8)).

$$\forall d \in \{SH, SC, DHW\}, \dot{Q}_{b,d}^{sys}(t) = A_b^{sys} \dot{Q}_{b,d}^{A}(t) \quad (8)$$

A thermal network links every buildings b with each other and with the central production plant (CPP, see Figure *1*). The effective width w_{net} (Persson et al.[25], Equation (10)) defines its length L_{net}(Equation (9)).

$$L_{net} = \frac{A^{grd}}{w_{net}} \quad (9)$$

$$w_{net} = min(137.5e + 5{,}60) \quad (10)$$

The definition of the network length assumes that the system plot ratio e is computed as if all buildings in the city were connected to the network. If buildings are evenly distributed in the city, the marginal network length to connect an additional building is negligible and the hypothesis is correct.

2.2.3 Temporal approach

The use of an hourly time step comes with high solving time. Thus, a smaller variable time step vector TSV_{var} is constructed from the base hourly time step vector TSV_{hourly}. For each element t of TSV_{hourly}, the two following rules are observed:

- Regular pavement: Given $t_{reg} > 1h$ an integer, if t_{reg} divides t then t is kept in TSV_{var}.
- Peak conservation: For each parametric time series p (demand, external temperature, etc.), if Equations (*11*) and (*12*) are verified, t and t-1 are kept in TSV_{var}. pc_{peak}^{min} and pc_{peak}^{max} are two percentiles of p.

$$p(t') \leq p_{pc_{peak}^{min}} \quad (11)$$

$$p(t') \geq p_{pc_{peak}^{max}} \quad (12)$$

The correctness of power balances using $TSV_{var}$is achieved by averaging each time series. This temporal approach reduces solving time but remains accurate (see Appendix 6.3). It is similar to the one adopted in Kouhia et al. [10] where the duration curve of the DH load profile is aggregated in seven periods. The absence of storage component in their model enables this break in time series continuity.

2.2.4 Components

A set of production (*prod*), storage (*stor*) and distribution network components are defined hereafter. Other components may be defined but these are the main technologies encountered in actual thermal systems. Bold font highlights optimization variables.

Table *2* presents the models of production components, which are linear. The nomenclature associates production component with the vectors they rely on. For instance, the term Abs^{drive}-HP^{sink}_{source} refers to an absorption heat-pump, driven by thermal vector *drive,* that moves heat from the thermal vector *source* to the thermal vector *sink*.

Table 2: Production components and their associated model.

Type	Technology	Nomenclature	Performance model
Boiler	Natural gas (condensing)	$Gas\text{-}Boil^{sink}$	Graphical reading, gas type H [26]
	Biomass (condensing)	$Biom\text{-}Boil^{sink}$	Graphical reading [27]
	Electric	$Elec\text{-}Boil^{sink}$	Constant efficiency $\eta_{Elec-Boil} = 100\%$
CHP – back-pressure	Natural gas (combined cycle)	$Gas\text{-}CHP^{sink}$	Full model [13], adapted for variable efficiency using boilers' models
	Biomass	$Biom\text{-}CHP^{sink}$	
Heat pump and chiller	Compression	$Comp\text{-}HP^{sink}_{source}$	Full model [28] Fluid: ammonia, $\eta_{is} = 0.75$ and $f_Q = 0.2$. Pinch temperature: 3K
	Absorption	Abs^{drive}-HP^{sink}_{source}	Full model [29] Pinch temperatures: 3K
Other	Flat plate solar thermal	STh^{sink}	See Appendix 6.2.1.
	Heat exchanger	HEx^{sink}_{source}	Constant efficiency $\eta_{HEx} = 95\%$
	Dry cooler	DRC^{sink}_{source}	See Appendix 6.2.2.
	Network pump	$Pump$	See Equation *(15)*

Two types of sensible thermal energy storage are used:

- Short-Term Thermal Energy Storage (STTES) is directly connected to other components.
- Long-Term Thermal Energy Storage (LTTES) stores energy using a storage-dedicated medium. The storage is charged (resp. discharged) using a heat exchanger (resp. compression HP).

Both of these storages are characterized by:

- An hourly losses rate $\epsilon_{stor}(\%/h)$.
- A minimum charge-discharge delay $\Delta t_{stor}(h)$.
- A maximum volume capacity $\boldsymbol{V^{sizing}_{stor}}$ (L).

A two-pipes distribution network links the CPP and the buildings. The operating temperatures are the same at every hub of the network and energy can flow both ways between two given hubs. Equation (13) and (14) present respectively the network energy balance and thermal exchanges between the network and the soil.

$$\dot{\boldsymbol{Q}}_{\boldsymbol{net,CPP}}(\boldsymbol{t}) = \dot{Q}_{net,loss}(t) + \sum_{b} \dot{\boldsymbol{Q}}_{\boldsymbol{net,b}}(\boldsymbol{t}) \tag{13}$$

$$\dot{Q}_{net,loss}(t) = L_{net} U \left(\frac{T_{net}^{hot}(t) + T_{net}^{cold}(t)}{2} - T_{soil}(t) \right) \quad (14)$$

Pump components cover pressure distribution losses at a given hub $h$that exchanges a power$\dot{\boldsymbol{Q}}_{\boldsymbol{net,h}}(\boldsymbol{t})$with the network. These losses should be proportional to $\left(\frac{\dot{Q}_{net,h}(t)}{\Delta T_{net}(t)}\right)^3$ but only a $\dot{\boldsymbol{Q}}_{\boldsymbol{net,h}}(\boldsymbol{t})$ dependency is kept for linearity reasons. Equation (*15*) presents the electrical consumption of a pump component.

$$\dot{\boldsymbol{E}}_{\boldsymbol{h,pump}}(\boldsymbol{t}) = p_{pump} \dot{\boldsymbol{Q}}_{\boldsymbol{net,h}}(\boldsymbol{t}) \quad (15)$$

The sizing variable of network components (length L_{net}) is a parameter, while $\boldsymbol{CAPEX_{net}}$ is an optimization variable. The operation variable is the annual energy$\boldsymbol{Q_{net,CPP}}$.

$\boldsymbol{CAPEX_{net}}$(€/m) depends on the average diameter of pipes in the network $\boldsymbol{D_{net}}$ (Persson et al. [25]). $\boldsymbol{D_{net}}$is a function of the network linear density and is determined using a piecewise linear approximation of Equation (*17*).The square root in Equation (*16*) adaptsΔT_{net}assuming the original correlation is valid for $\Delta T_{net} = 50K$.

$$\boldsymbol{CAPEX_{net}} = 212 + 4464 \sqrt{\frac{50}{min(\Delta T_{net})}} \boldsymbol{D_{net}} \quad (16)$$

$$\boldsymbol{D_{net}} = max\left(0.0486\, ln\left(\frac{\boldsymbol{Q_{net,CPP}}}{L_{net}}\right) + 0.0007, 0.02\right) \quad (17)$$

$\boldsymbol{F_{b,v}(t)}$ **and** $\boldsymbol{F_{CPP,v}(t)}$ in Figure *1* are power flows between a hub and the surrounding system. These flows occur in EnergyIO components and are related to vector v. They make GHG emissions (parameter $CC_v(t), kgEqCO_2/kWh$) and exergy potential $\left(EX_v(t)\right)$ enter or leave the energy system. $EX_v(t)$ depends on an exergy reference temperature T_0 for vectors v other than electricity.

The flow $\boldsymbol{F_{h,v}}$ is associated to an energy cost$OPEX_{V_{h,v}}$and can be constrained in terms of capacity and annual energy availability. Thermal demands$Q_{b,d}^{sys}$are a particular case of such flows for which cost $OPEX_{V_{h,v}}$ and carbon content CC_v are zeros.

Equation (*18*) is a constraint added to the model to ensure that the peak DHW demand could be met using the installed production and storage components at building level. Let $P_{b,DHW}$, respectively $S_{b,DHW}$, be the set of production components, respectively storage, in building b, that satisfy the DHW demand.

$$\dot{Q}_{b,DHW}^{sizing} = \sum_{prod \in P_{b,DHW}} \dot{\boldsymbol{Q}}_{\boldsymbol{prod}}^{\boldsymbol{sizing}} + c_p \min(\Delta T_{DHW}) \sum_{stor \in S_{b,DHW}} \frac{\boldsymbol{V}_{\boldsymbol{stor}}^{\boldsymbol{sizing}}}{\Delta t_{stor}} \quad (18)$$

Note that the probability of simultaneous DHW power peaks at the city scale is low, thus constraint (18) is not extended to CPP.

2.2.5 Objective functions

An energy system can be optimal according to one of the following independent objective functions:

- The LCOE ($€/kWh$) (see Equation (19)) comprises the cost of investment and operation of production, storage, energyIO and network components.

$$\boldsymbol{LCOE} = \frac{\sum_{net} \boldsymbol{C_1(net)} + \sum_h \sum_{c \in h} \boldsymbol{C_2(c)}}{\left(\sum_b \sum_d Q_{b,d}^{sys}\right) \times \sum_1^{n^{sys}} (1 + r^{sys})^{-y}} \tag{19}$$

Equations (20) and (21) define the helper function $\boldsymbol{C_2}$.Sizing variable of production components $\boldsymbol{\dot{Q}_c^{sizing}}$is their maximal thermal capacity, except for CHP and pump components (electrical capacity $\boldsymbol{\dot{E}_{prod}^{sizing}}$is used) and for solar thermal (solar field area $\boldsymbol{A_{prod}^{sizing}}$is used). The operation variable $\boldsymbol{Q_c}$ is the annually produced energy. Storage components do not define $\boldsymbol{Q_c}$.

$$\boldsymbol{C_2(c)} = \sum_{\boldsymbol{y=1}}^{n^{sys}} \left[CAPEX_c\left(rep_c(y) + OPEX_{F_c}\right) \times \boldsymbol{\dot{Q}_c^{sizing}} + OPEX_{V_c} \times \boldsymbol{Q_c} \right] (1 + r^{sys})^{-y} \tag{20}$$

$$rep_c(y) = \begin{cases} 0 \; if \; \forall q \in \mathbb{N}, y - 1 \neq q \times n_c \\ min\left(\frac{n^{sys} - (y-1)}{n_c}, 1\right) else \end{cases} \tag{21}$$

The network cost is evaluated with a function C_1 similar to C_2except that the sizing element is L_{net} while the CAPEX is $\boldsymbol{CAPEX_{net}}$(Equation (16)).

- The operational CO_2 emissions ($kgEqCO_2/MWh$) is defined in Equation (22):

$$\boldsymbol{CC} = \frac{\sum_h \sum_v \sum_t CC_v(t) \boldsymbol{F_{h,v}(t)}}{\sum_b \sum_d Q_{b,d}^{sys}} \tag{22}$$

- The operational exergy losses (MWh/MWh) is defined in Equation (23). The numerator covers every valuable exergy flow entering or exiting the system including the thermal demand. It excludes air-related energy transfer and energy losses in distribution networks.

$$\boldsymbol{EX} = \frac{\sum_h \sum_v \sum_t EX_v(t) \boldsymbol{F_{h,v}(t)} + \sum_b \sum_v \sum_t EX_d(t) Q_{b,d}^{sys}(t)}{\sum_b \sum_d Q_{b,d}^{sys}} \tag{23}$$

2.3 Performance indicators

Each energy system is optimized according to the three objective functions defined in Equations (19), (22) and (23) (one at a time). These are also considered performance indicators.

Two centralization rates quantify the use of centralized architectures. One is defined regarding sizing capacity (Equations (24)) of production components, the other depends on annual energy (Equation (25)). Note that network heat exchangers in SFH/MFH, network pumps and dry coolers components are excluded from this count.

$$\boldsymbol{CR^{sizing}} = \frac{\sum_{prod \in CPP} \boldsymbol{\dot{Q}_{prod}^{sizing}}}{\sum_{prod \in \{CPP,SFH,MFH\}} \boldsymbol{\dot{Q}_{prod}^{sizing}}} \tag{24}$$

$$\boldsymbol{CR^{energy}} = \frac{\sum_{prod \in CPP} \boldsymbol{Q_{prod}}}{\sum_{prod \in \{CPP,SFH,MFH\}} \boldsymbol{Q_{prod}}} \tag{25}$$

3 Case study

The model described previously is used to map the economic, environmental, and exergy performances of four thermal architectures in four contexts.

3.1 Case specific parameterisation

3.1.1 Thermal demands

This study considers two countries for their opposite climate, yet the optimization model (part 2.2) is not country-specific.

Weather data[31]and solar position vector [32] for Roma and Stockholm are used. For each country, low (NR, code 001 in Tabula Episcope) and high (HR, code 003) thermal retrofitting levels of buildings are considered. The retrofitting affects the thermal demand (defined in Section2) and SH and SC thermal emitters (Table *3*). Water circulating in each thermal emitter is either cooled or warmed by indoor air. This water temperature varies along the year for SH demand in NR buildings.

Table 3: Temperatures of thermal emitters for SH and SC demands
(see the nomenclature for NR / SH case notation)

	SH		SC	
	$T_{SH}^{hot}\ (°C)$	$T_{SH}^{cold}(°C)$	$T_{SC}^{cold}\ (°C)$	$T_{SC}^{hot}\ (°C)$
NR	$(-15, 80) \xrightarrow{T_{air}} (15, 40)$	35	7	12
HR	35	25	15	20

Table 4 gives the set point air temperature associated to each demand. The return temperature of the DHW system$T_{DHW}^{cold}$is a weighted average of draw-off (cold water temperature in *Table 1*) and recirculation contributions (55 °C).

Table 4: Set points temperatures for all demands

SH	SC	DHW	
$T_{SH}\ (°C)$	$T_{SC}\ (°C)$	$T_{DHW}^{hot}\ (°C)$	$T_{DHW}^{cold}\ (°C)$
20	$\forall t, \max(22, T_{air}(t) - 7)$[30]	60	36

Buildings are either single-family houses (SFH) or multi-family houses (MFH) (Table *5*). The city ground area (A^{grd}) is $10\ km^2$.

Table 5: Repartition and properties of residential buildings by size

	Plot ratio e_b	Proportion p_b (%)
SFH	0.3	25
MFH	0.5	75

Given a country, size and retrofitting level, the construction period information in the Tabula database must be aggregated to model a unique theoretical average building:

1. Data about national building stocks per construction year is collected[33].
2. The cumulative distribution of this data set is calculated.
3. The shares of the building stock per Tabula period of construction year is inferred from 2.

An hypothesis is that the construction year data provided by [33] is valid and the same for all(building size; retrofitting level) pairs. The thermal demands of an average theoretical building are weighted averages of the demands of its constituting real buildings.

3.1.2 Architectures

Five major thermal architectures are defined hereafter. Each one is a set of production, storage and network components that are consistent with each other and able to satisfy one, two or three of the thermal demands.

- The no-network architecture: production and storage are fully decentralized.
- The 2GDH architecture: 2nd generation DH network with absorption chillers for local cold production.
- The 4GDHarchitecture: 4th generation DH network.
- The DC architecture: typical district cooling network with active cold production in CPP.
- The 5GDHC architecture: bidirectional near-ambient temperature two-pipe network [34].

A complete description of these architectures is given in Table 6. Note that each air-sourced or air-cooled Comp-HP is used with a DRC component and air-sourced Comp-HP are disabled when $T_{air} < 0°C$.

Table 6: Properties of the five thermal architectures.

[a)] NR buildings only. The "+" operator stands for a series assembly at the pivot temperature $T = 60°C$.
[b)] HR buildings only [c)] Water is warmed from 90 to 100 °C [d)] Shared with series assemblies if applicable.

		NN	2GDH	4GDH	5GDHC	DC
SFH/MFH	SH	$Comp\text{-}HP_{air}^{SH}$ + $Gas\text{-}Boil^{SH a)}$ $Comp\text{-}HP_{air}^{SH}$ + $Elec\text{-}Boil^{SH a)}$ $Elec\text{-}Boil^{SH d)}$ $Gas\text{-}Boil^{SH d)}$ $Comp\text{-}HP_{air}^{SH b)}$	HEx_{net}^{SH}	HEx_{net}^{SH} + $Gas\text{-}Boil^{SH a)}$ HEx_{net}^{SH} + $Elec\text{-}Boil^{SH a)}$ $HEx_{net}^{SH\ b)}$	$Comp\text{-}HP_{net}^{SH}$ + $Gas\text{-}Boil^{SH a)}$ $Comp\text{-}HP_{net}^{SH}$ + $Elec\text{-}Boil^{SH a)}$ $Comp\text{-}HP_{net}^{SH b)}$	
	SC	$Comp\text{-}HP_{SC}^{air}$	$Abs^{net}\text{-}HP_{SC}^{air}$		$Comp\text{-}HP_{SC}^{net\ a)}$ $HEx_{SC}^{net\ b)}$	HEx_{SC}^{net}
	DHW	$Elec\text{-}Boil^{DHW}$ $Gas\text{-}Boil^{DHW}$ $Comp\text{-}HP_{air}^{DHW}$ STh^{DHW} $STTES_{DHW}$	HEx_{net}^{DHW} $STTES_{DHW}$	HEx_{net}^{DHW} $STTES_{DHW}$	$Comp\text{-}HP_{net}^{DHW}$ $STTES_{DHW}$	
Network	T_{hot}^{net} $(°C)$		$(-15, 140) \xrightarrow{T_{air}} (15, 100)$	63	17	9
	T_{cold}^{net} $(°C)$		70	40	7	4
	p_{pump}		0.5% (CPP level)	0.5% (CPP level)	5% (building level)	0.5% (CPP level)
CPP	Heating		$Gas\text{-}CHP^{net}$ $Biom\text{-}CHP^{net}$ $Biom\text{-}Boil^{net}$ $Gas\text{-}Boil^{net}$ $HEx_{IEH_4}^{net}$	$Gas\text{-}CHP^{net}$ $Biom\text{-}CHP^{net}$ $Biom\text{-}Boil^{net}$ $Gas\text{-}Boil^{net}$ $Abs^{IEH_3}\text{-}HP_{IEH_1}^{net}$ $Abs^{IEH_4}\text{-}HP_{IEH_1}^{net}$ $Abs^{IEH_3}\text{-}HP_{IEH_2}^{net}$ $Abs^{IEH_4}\text{-}HP_{IEH_2}^{net}$ $Comp\text{-}HP_{IEH_1}^{net}$ $Comp\text{-}HP_{IEH_2}^{net}$ $HEx_{IEH_3}^{net}$ $HEx_{IEH_4}^{net}$ STh^{net}	$Abs^{IEH_3}\text{-}HP_{air}^{net}$ $Abs^{IEH_4}\text{-}HP_{air}^{net}$ $Comp\text{-}HP_{air}^{net}$ $HEx_{IEH_1}^{net}$ $HEx_{IEH_2}^{net}$ $HEx_{IEH_3}^{net}$ $HEx_{IEH_4}^{net}$	$Gas\text{-}CHP^{90/100 c)}$ $Biom\text{-}CHP^{90/100 c)}$
	Cooling				$Abs^{IEH_3}\text{-}HP_{net}^{air}$ $Abs^{IEH_4}\text{-}HP_{net}^{air}$ $Comp\text{-}HP_{net}^{air}$	$Abs^{IEH_3}\text{-}HP_{net}^{air}$ $Abs^{IEH_4}\text{-}HP_{net}^{air}$ $Abs^{90/100}\text{-}HP_{net}^{air}$ $Comp\text{-}HP_{net}^{air}$
	Storage		$STTES_{net}$	$STTES_{net}$ $LTTES_{10/60}$	$STTES_{net}$	$STTES_{net}$
Comments			Heat in CPP isproduced at 140°C no matter ΔT_{net}.Energy balance of$STTES_{net}$ is unfavorable.			Heat transfers from the network to the ground are not considered.

Four cases are defined by grouping architectures (Table *7*). For each case, the available components are the union of components of the constituting architectures. Thus, the cases NN_2G, NN_4G_DC and NN_5G will outperform the case NN.

Table 7: Architectures assemblies

Case	NN	NN_2G	NN_4G_DC	NN_5G
Architectures involved	NN	NN, 2GDH	NN, 4GDH, DC	NN, 5GDHC

3.2 Common parameterisation

3.2.1 Energy vectors

The CPP benefits from nearby industrial excess heat, in proportion of annual SH and DHW demands, according to Equation (26). This heat is available at four temperature levels and at a constant capacity along the year. Data regarding levels 1, 2 and 3 are inspired by the European project SEEnergies [35].

$$\forall t, \forall v \in \{IEH_1, IEH_2, IEH_3, IEH_4\}, \dot{F}_{CPP,v}(t) = \frac{p_v}{8760} \sum_b \sum_t (\dot{Q}^{sys}_{b,SH}(t) + \dot{Q}^{sys}_{b,DHW}(t)) \quad (26)$$

Table 8 shows the availability of IEH sources. The share of $\dot{F}_{CPP,v}(t)$ (Equation(26)) that is not used for thermal production must be dissipated in a DRC component.

Table 8: Temperatures and availability of IEH

Vector name	IEH_1	IEH_2	IEH_3	IEH_4
$T\ (°C)$	25	55	95	150
p_v (%)	6.0	2.3	1.7	5

Table *9* presents the properties of electricity, natural gas and biomass also used in the study.

Table 9: Properties of energy vectors

	Availability		$T_v\ (K)$
	SFH / MFH	CPP	
Electricity	Receiving	Receiving and emitting Hourly limit: 200 MW	NA $(EX_v(t) = 1)$
Natural gas	Receiving	Receiving	1963
Biomass	Not available	Receiving Annual limit: 250 GWh Hourly limit: 200 MW	1073

Exergy factors (Equation (27)) depend on the vector temperatureT_v and the ambient air temperature($T_0 = T_{air}$). It is worth mentioning that for each thermal demand d, T_v is the logarithmic mean of the emitter temperatures (T_d^{hot}, T_d^{cold}).

$$EX_v(t) = 1 - \frac{T_0(t)}{T_v(t)} \quad (27)$$

While IEH is free, costs for other energy vectors are given by Table *10*.

Table 10: Costs of energy vectors (€/MWh).
Taxes are not included.

	SFH/MFH			CPP		
	IT	SE	Source	IT	SE	Source
Electricity	122	102	nrg_pc_204, 41611904 (5000 to 15000 kWh) Year 2018[36]	67	41	nrg_pc_205, 4162906 (70 to 150 GWh) Year 2018[36]
Natural gas	54	68	nrg_pc_202, 4141902 (20 to 200 GJ) Year 2018[36]	25	34	nrg_pc_203, 4142904 (100 to 1000 TJ) Year 2018[36]
Biomass				36.1		[37]

Carbon contentsCC of natural gas and biomass are respectively 244 kgEqCO_2/MWh and 25.8 kgEqCO_2/MWh [38]. National average values are used regarding electricity([39], year 2018), i.e.416 kgEqCO_2/MWh for Italy and 52 kgEqCO_2/MWh for Sweden.

3.2.2 Components

Table *11* (resp.Table *12*) lists the economic properties of production components (resp. storage components).

Table 11: Properties of production components. Each 3-tuple is the value for hubs (CPP/MFH/SFH).
a) Lack of data b) Air-sourced or air-cooled heat pump, CPP only c) Reference vector is electricity, d) In $€/m^2$

	$CAPEX$ $(€/kW)$	$OPEX_F$ $(\%CAPEX/yr)$	$OPEX_V$ $(€/MWh)$	n $(year)$	Source
$Gas\text{-}Boil^{sink}$	$(60, 61.5, 310)$	$(3.25, 2.72, 6.61)$	$(1.1, 0, 0)$	(25,25,20)	[40], [27]
$Biom\text{-}Boil^{sink}$	$(710, -, -)$	$(4.59, -, -)$	$(1.98, -, -)$	$(25, -, -)$	[27]
$Elec\text{-}Boil^{sink}$	$(-$,644,967)	$(-$,0.05,0.83)	$(-$,0,0)	30	[40]
$Gas\text{-}CHP^{sink_{c)}}$	$(900, -, -)$	$(3.33, -, -)$	$(4.5, -, -)$	25	[13]
$Biom\text{-}CHP^{sink_{c)}}$	$(2000, -, -)$	$(2.85, -, -)$	$(2, -, -)$	40	[13]
$Comp\text{-}HP^{sink}_{source}$	$(1240, 352.5, 940)$ $860^{b)}$	$(0.16, 1.17, 2.96)$ $2.32^{b)}$	$(2.7, 0.47, 0)$ $1.7^{b)}$	$(25, 20, 18)$ $25^{b)}$	[40], [27]
$Abs^{drive}\text{-}HP^{sink}_{source}$	$(560, 332, 1458)$	0.36	1	25	Internal, [27]
STh^{sink}	$(187,405,600)^{d)}$	(0.04,0.48,1.89)	(0.21,0,0)	(30,25,25)	[40], [27]
HEx^{sink}_{source}	$(100, 265, 265)$	0	1.5	40	[41]
$Pump^{c)}$	90	$0^{a)}$	$0^{a)}$	$10^{a)}$	[41]

Flat plate solar thermal capacity is bounded using the max collector area $\overline{A^{sizing}_{STh}}$:

- For CPP, $\overline{A^{sizing}_{STh}} = 50000m^2$.
- For SFH/MFH, $\overline{A^{sizing}_{STh}}$ is half the roof area of the building (sum of 'A_roof_1' and 'A_roof_2' attributes in the Tabula database[19]).

SFH/MFH benefits from DHW storage. Equation (*28*) gives the maximum storage volume, in L/m^2, as a function of the number of living units and the area of the building [21].

$$\overline{V^{A,sizing}_{b,stor}} = \frac{15.5 \times n_{b,apartments} + 156}{A_b} \tag{28}$$

Table 12: Properties of storage components.
a) Adaptation of original data

Description	Hub	Technical parameters			Economic parameters			Source
		Charge/discharge delay (h)	Energy losses (%/h)	Capacity (m^3)	$CAPEX$ $(€/m^3)$	$OPEX_F$ $(\%CAPEX/yr)$	n $(year)$	
$STTES$	SFH/MFH	$1^{a)}$	2.1	Upper bound given by Equation(28)	14280	4.07	30	[42]
	CPP	60	0.0834	$3e3$ (upper and lower bounds)	173	0.29	40	[42]
$LTTES$	CPP	968	$0^{a)}$	$500e3$ (upper and lower bounds)	26.2	0.52	20	[42]

The parameters associated with thermal networks are given by Table *13*.

Table 13: Properties of the network component

U $(W/(K.m))$	T_{soil} $(°C)$	$OPEX_{F_{net}}$ $(\%CAPEX/yr)$	$OPEX_{V_{net}}$ $(€/MWh)$
0.7	[43] – one meter depth	0.06	1.5

Moreover, a 75% reduction of $\boldsymbol{CAPEX_{net}}$ stands for public incentives to DH and DC.

3.2.3 Selection of a temporal approach

Based on the results presented in Appendix 6.3, the parameters for time step selection are $t_{reg} = 2$, $p_{pc_{peak}^{min}} = 0.011\%$(only the index of minimum value) and $p_{pc_{peak}^{max}} = 100\% - 0.011\%$ (only the index of maximum value).The selection of the time vector is based on the following time series:

- For each building, the thermal demands SH, SC, DHW, sum of SH and SC, sum of SH and DHW, sum of SC and DHW.
- External and soil temperatures, solar irradiance.

Note that five additional time steps are selected according to a third method, which is not detailed here.

This leads to approximately 4400 time intervals in TSV_{var} (instead of 8760 in TSV_{hourly}).

3.3 Execution details

In total, 48 cases are defined using 4 architectures, 2 countries, 2 levels of thermal retrofitting and 3 objective functions. These are run in parallel on a machine with processor Intel Xeon Gold 6154 and 96 GB memory. The optimization process takes about 5 hours with an optimality gap of 0.5%.

4 Results

4.1 Global trends

The continuous indicators values (part 2.3) are discretized according to Figure *2*.

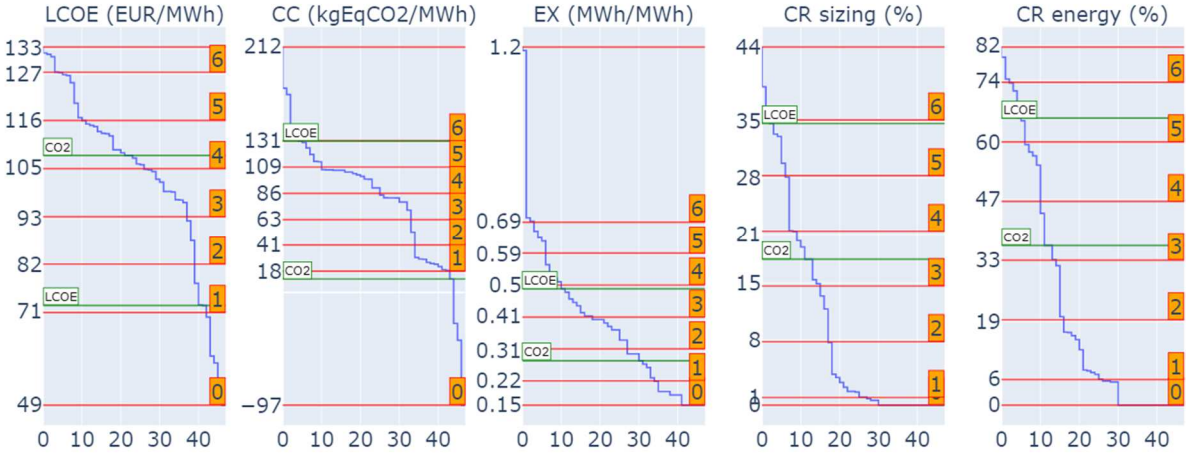

Figure 2: Indicators values for each of the 48 cases. The lower the better regarding LCOE, CC and EX.
Orange bars describe discretization used in Figure 3.
Labels CO2 and LCOE refer to the case detailed in part 4.2.

Figure *3*presents the discretized indicators in radar charts. Results comment is performed on continuous data.

Best technological choices depend on the objective function that is minimized. Since in Sweden electricity is cheaper than gas, the best LCOE minimization is achieved by architecture NN_4G_DC using compression HP. On average $LCOE = 71\,€/MWh$ (NR and HR scenarios). In Italy, NN_2G is the most profitable architecture ($LCOE = 49\,€/MWh$) thanks to a$Gas\text{-}CHP$unit being intensively used. Its production during summer drives absorption chillers at SFH/MFH level. Regarding DC architecture, the profitability of a $Gas\text{-}CHP$unit driving an absorption chiller at CPP level does not balance the costs and thermal losses associated with the distribution infrastructure.

Regarding CO_2 minimization, NN_4G_DC and NN_2Gperform the best since the electricity production of their CHP units is sent on the grid with the equivalent CO_2 emissions being deduced. Italy and HR cases particularly

benefit from this effect due to respectively high carbon content of electricity and low thermal demand compared to annual biomass limitation (see Table *9*).

Italy outperforms Sweden regarding EX minimization. Indeed, when $T_{air} < 0°C$, which is common in Sweden, boilers with low exergy efficiency must be used instead of heat pumps. In Sweden, NN_4G_DC and NN_5G achieves a 30% and 8.1% reduction in EX value compared to NN, thanks to solar thermal (NN_4G_DC only), low network losses and advanced IEH use. EX is 11% smaller in HR cases compared to NR cases thanks to lower SH and high SC emitters temperatures.

This case study reveals common trends of typical DH and DC systems but relies on significant hypothesis:

- The subsidized distribution network promotes network architectures (LCOE minimization) while a low availability of low-grade heat (IEH) penalizes them (especially5GDH architecture).
- Energy exchanges account up to 50% of the LCOE and yet rely on inherently uncertain costs (Table *10*.).

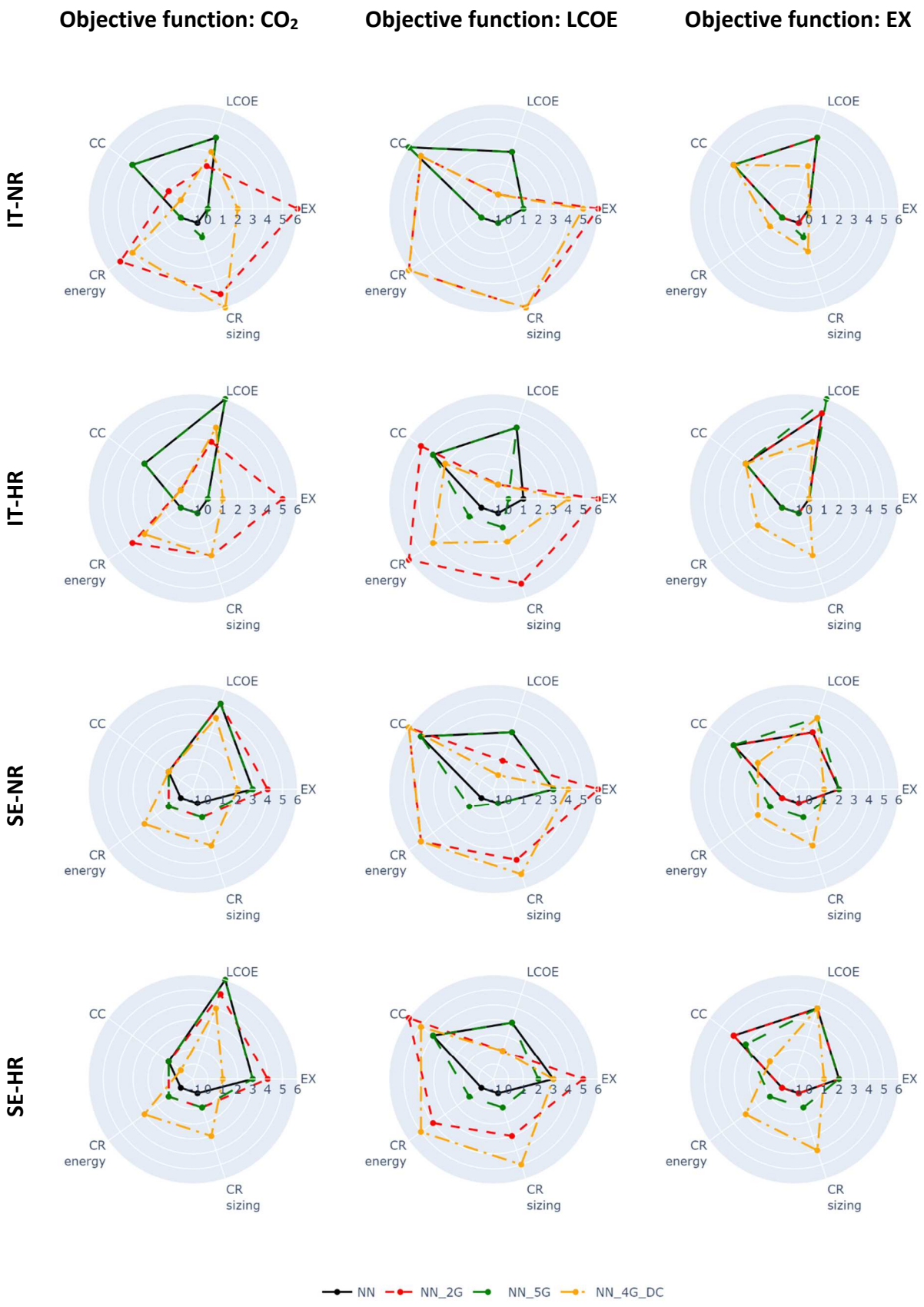

Figure 3: Discretized values of the performance indicators.
Each row of charts is a scenario. Each branch of a given chart is a performance indicator.

4.2 Focus on a particular case

Particular attention is now drawn to the case SE-HR for architecture NN_4G_DC. Figure 4describes heat production per hub and component. Some data in Figure 4 are aggregated (IEH-related components, peak and stand-alone SH boilers) and values lower than 100 MWh are removed. Values of performance indicators are reported in Figure *2*.

A transition from LCOE-based to CO2-based minimization reduces theCO2 emissions by 91% and increases the energy cost by 49% (Figure *2*). The corresponding cost of avoided carbon emissions is $297\ €/tEqCO_2$.

Figure 4: Annual energy production of each component. Scenario (SE-HR) for the architecture NN_4G_DC. Each row of charts refers to an energy hub.

The base heat production in CPP is met by a gas boiler (resp. biomass CHP) for LCOE (resp. CO_2) minimization (Figure 4). In CO_2-minimization the long-term storage covers a large part of the network heating load as annual energy limit on biomass is reached. Regarding SC, low electricity cost in CPP makes DC the least cost solution for SFH while MFH takes advantage of the low $CAPEX$ of its chiller. Yet, the least CO_2-emitting solution remains individual chillers since the network temperatures are low ($T^{net} = (4, 9)°C$) compared to the emitters temperatures ($T_{SC} = (15, 20)°C$), leading to low COP of CPP chiller.

DHW demand is mostly satisfied by the compression heat pump ($Comp\text{-}HP_{air}^{DHW}$). Decentralized solar thermal is used only in CO_2-minimization. Conversely, only in LCOE-minimization (MFH), a gas boiler prevents the over-

sizing of the heat pump (peak demand) and its operation in unfavorable conditions (cold nights), which are situations that would lead to respectively high investment and high operating costs.

Figure 5 presents the 4GDH heat production in CPP, per component. IEH absorption HP cover a base 5 MW power and are generally preferred over heat exchangers to enhance high temperature IEH as their COP is higher than 1. In CO2 minimization, solar production (hour 2260 and onward in Figure 5) either is stored or directly feeds the network. One third of the energy capacity of LTTES is never used (Table *12* recalls that this capacity is constrained on a fixed value). The storage is discharged during winter to relieve $Biom\text{-}CHP$.

Figure 5: Duration curve of the thermal power carried by the 4GDHnetwork.
*S*cenario (SE-HR) for the architecture NN_4G_DC.
Except the discharge of LTTES, the missing representation of storage explains the discrepancies between the black line (network load) and colored area (production).

5 Conclusion and outlook

The energy transition faces the double challenge of phasing out fossil fuels and satisfying an increasing cooling demand. Concomitantly, previous works showed that multiple technologies can be genuinely combined to meet SH, SC and DHW demands in the context of this transition. The framework presented in this article facilitates the comparison of these technologies. It is based on two independent parts.

A demand model generates SH, SC and DHW profiles given simple building construction properties and hourly meteorological data. DHW demand is also defined by its sizing thermal power, i.e. the maximum demand production and storage systems must be able to meet occasionally.

An optimization model reveals the best technological choices to meet these demands. It follows the MILP formalism and is based on an energy hub approach. Three types of objective functions are considered, namely LCOE, operating GHG emissions and exergy efficiency. Near-LP component models and spatial complexity reduction make possible the fast comparison of several thermal architectures.

A case study involving Swedish and Italian contexts shows, for instance, the effect of harsh climates on sizing of production components.

Overall, it appears that this framework is a step forward to the modelling of multi-vector city-scale energy system, though with a trade-off on accurate system operation.

6 Appendix

6.1 Validation of the demand model

The city of Brussels is used as a reference for weather data [44] and solar position vector [32] in adapted model. Results show that only 6 buildings out of 99 are such that the annual SH demand calculated with the adapted model differ by more than 5% from the Tabula model.

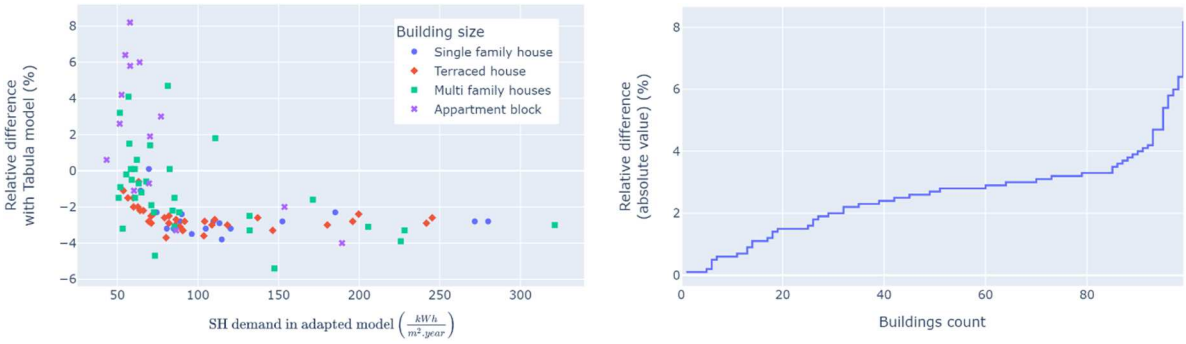

Figure 6: Difference in annual SH demand between Tabula and adapted models as a function of SH demand (left), cumulative distribution of this difference (right).

6.2 User-defined MILP components

6.2.1 Flat plate solar thermal

The following hypotheses are made regarding the solar field$p$:

- Orientation is such that annual irradiance $I(t)$ is maximized (data [31]).
- Connection to the energy system through a heat exchanger, with $\Delta T^{pinch} = 3K$.
- Use of standard coefficients η_0, a_1, a_2 and a_5 (data [45]).

Equation (*29*) gives the mean temperature of the heat medium circulating in the solar field. T^{cold} and T^{hot} are the temperatures of the cold side of the exchanger.

$$T_p(t) = \frac{T_p^{cold}(t) + T_p^{hot}(t)}{2} + \Delta T^{pinch} \tag{29}$$

Two kinds of losses are taken into account:

- Solar field medium to the air, Equation (*30*).

$$Q_{p,loss}^{A}(t) = a_1 \times \left(T_p(t) - T_{air}(t)\right) + a_2 \times \left(T_p(t) - T_{air}(t)\right)^2 \tag{30}$$

- Solar field panels to the air, Equation (*31*). These losses occur on a longer time scale than medium losses thus are distributed over the heat production profile $Q(t)$ (Equation (*32*)).

$$Q_{p,inertia}^{A} = a_5 \times \frac{\sum_t \left(T_p(t) - T_{air}(t)\right)}{8760} \tag{31}$$

$$\boldsymbol{Q_p(t)} = \boldsymbol{A_p^{sizing}} \times max\left(\eta_0 \times I(t) - Q_{p,loss}(t) - Q_{p,inertia}^{A}, 0\right) \tag{32}$$

The solar field area $\boldsymbol{A_P^{sizing}}$ is constrained by a maximal area $\overline{A_p^{sizing}}$ (Equation (33)).

$$\boldsymbol{A_p} \leq \overline{A_p} \tag{33}$$

6.2.2 DryCooler

The DryCooler component (DRC) facilitates thermal power exchanges between a water flow and ambient air using electricity-powered fans which electrical consumption is proportional to the energy being dissipated

(Equation (*34*)), i.e. $\eta_{DRC} = 2.75\%$. To account for the inefficiency of the transfer, the water flow must be $7°C$ higher (resp. lower) than air temperature if it is cooled (resp. warmed).

$$\boldsymbol{E_{elec,p}(t)} = \eta_p \times \boldsymbol{Q_p(t)} \quad (34)$$

6.3 Validation of the temporal approach

The validation follows two steps:

1. Minimization of the LCOE of a given energy system (sizing, operation) for different time step approaches (Table *14*). Three parameters families are defined:
    a. *regular* (R): A regular pavement of value t_{reg} is considered.
    b. *both low* (BL):In addition to the regular pavement,0.5% of the smallest and 0.5% of the largest values in each time series profile$p$ are considered.
    c. *both high* (BH): Same than BL with 1% of the smallest and 1% of the largest values in p.

Table 14: Validation methodology of the variable time step approach

	Case R1	Case R6	Case R24	Case BL6	Case BL24	Case BH6	Case BH24
t_{reg}	1	6	24	6	24	6	24
pc_{peak}^{min}	0	0	0	0.005	0.005	0.01	0.01
pc_{peak}^{max}	1	1	1	0.995	0.995	0.99	0.99

2. Comparison in objective value and deterministic time of each case with R1 case (reference).

The results show that BH and BL cases achieve interesting trades-off between accuracy and solving time (Figure *7*).

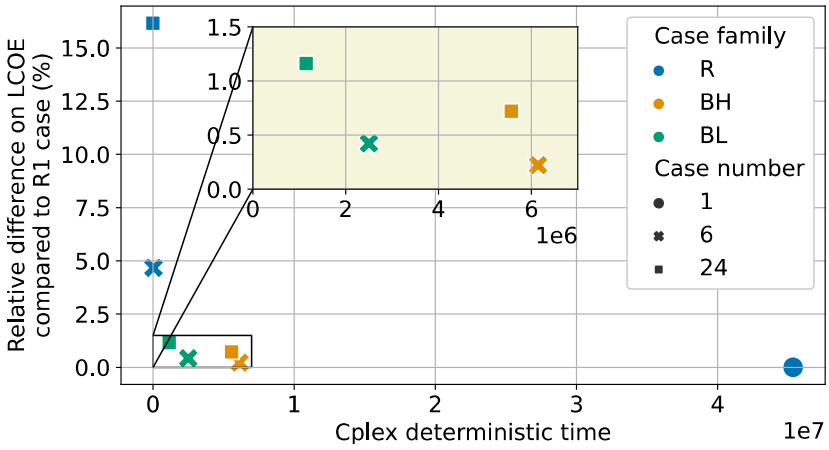

Figure 7: Accuracy of different temporal approaches as a function of solving time.

6.4 Case study thermal demand

Figure *8* presents the case study thermal demands as a function of the city ground area $A^{grd} = 10\ km^2$. Note that the thermal area is$A^{sys} = e \times A^{grd} = 4.3\ km^2$. Typical meteorological years [31] describe actual climate conditions.

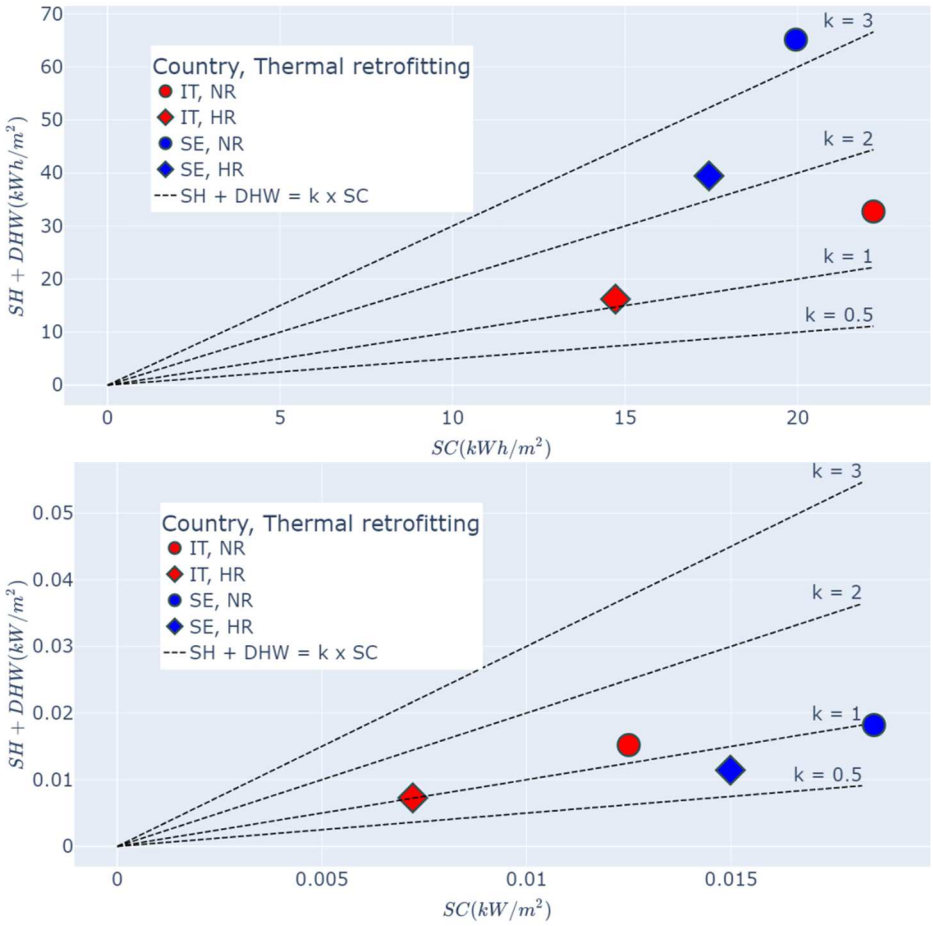

Figure 8: Annual thermal energy demands (top) and peak powers (bottom) (SFH/MFH buildings)

7 Acknowledgments

The support of ADEME (French Environment and Energy Management Agency) is gratefully acknowledged.

8 References

[1] International Energy Agency. The Future of Cooling: Opportunities for energy efficient air conditioning. Paris: IEA; 2018.

[2] Paris Agreement 2015. https://ec.europa.eu/clima/eu-action/international-action-climate-change/climate-negotiations/paris-agreement_en (accessed March 30, 2022).

[3] Lund H, Werner S, Wiltshire R, Svendsen S, Thorsen JE, Hvelplund F, et al. 4th Generation District Heating (4GDH): Integrating smart thermal grids into future sustainable energy systems. Energy 2014;68:1–11. https://doi.org/10.1016/j.energy.2014.02.089.

[4] Wirtz M, Hahn M, Schreiber T, Müller D. Design optimization of multi-energy systems using mixed-integer linear programming: Which model complexity and level of detail is sufficient? Energy Conversion and Management 2021;240:114249. https://doi.org/10.1016/j.enconman.2021.114249.

[5] Casisi M, Buoro D, Pinamonti P, Reini M. A comparison of different district integration for a distributed generation system for heating and cooling in an urban area. Applied Sciences (Switzerland) 2019;9. https://doi.org/10.3390/app9173521.

[6] Lazzeroni P. Design of a polygeneration system with optimal management for a dhc network. International Journal of Sustainable Energy Planning and Management 2019;22. https://doi.org/10.5278/ijsepm.2450.

[7] Fahlén E, Trygg L, Ahlgren EO. Assessment of absorption cooling as a district heating system strategy – A case study. Energy Conversion and Management 2012;60:115–24. https://doi.org/10.1016/j.enconman.2012.02.009.

[8] Chardon G, Le Pierrès N, Ramousse J. On the opportunity to integrate absorption heat pumps in substations of district energy networks. Thermal Science and Engineering Progress 2020;20:100666. https://doi.org/10.1016/j.tsep.2020.100666.

[9] Bartolozzi I, Rizzi F, Frey M. Are district heating systems and renewable energy sources always an environmental win-win solution? A life cycle assessment case study in Tuscany, Italy. Renewable and Sustainable Energy Reviews 2017;80:408–20. https://doi.org/10.1016/j.rser.2017.05.231.

[10] Kouhia M, Laukkanen T, Holmberg H, Ahtila P. Evaluation of design objectives in district heating system design. Energy 2019;167:369–78. https://doi.org/10.1016/j.energy.2018.10.170.

[11] Stanley Lee E, Li RJ. Fuzzy multiple objective programming and compromise programming with Pareto optimum. Fuzzy Sets and Systems 1993;53:275–88. https://doi.org/10.1016/0165-0114(93)90399-3.

[12] Morvaj B, Evins R, Carmeliet J. Optimising urban energy systems: Simultaneous system sizing, operation and district heating network layout. Energy 2016;116:619–36. https://doi.org/10.1016/j.energy.2016.09.139.

[13] Dahl M, Brun A, Andresen GB. Cost sensitivity of optimal sector-coupled district heating production systems. Energy 2019;166:624–36. https://doi.org/10.1016/j.energy.2018.10.044.

[14] Dzenajavičienė EF, Kveselis V, McNaught C, Tamonis M. Economic analysis of the renovation of small-scale district heating systems—4 Lithuanian case studies. Energy Policy 2007;35:2569–78. https://doi.org/10.1016/j.enpol.2006.09.009.

[15] Jangsten M, Filipsson P, Lindholm T, Dalenbäck J-O. High Temperature District Cooling: Challenges and Possibilities Based on an Existing District Cooling System and its Connected Buildings. Energy 2020;199:117407. https://doi.org/10.1016/j.energy.2020.117407.

[16] Swing Gustafsson M, Myhren JA, Dotzauer E. Life Cycle Cost of Heat Supply to Areas with Detached Houses—A Comparison of District Heating and Heat Pumps from an Energy System Perspective. Energies 2018;11:3266. https://doi.org/10.3390/en11123266.

[17] Best RE, Rezazadeh Kalehbasti P, Lepech MD. A novel approach to district heating and cooling network design based on life cycle cost optimization. Energy 2020;194:116837. https://doi.org/10.1016/j.energy.2019.116837.
[18] Geidl M, Koeppel G, Favre-Perrod P, Klockl B, Andersson G, Frohlich K. Energy hubs for the future. IEEE Power and Energy Magazine 2007;5:24–30. https://doi.org/10.1109/MPAE.2007.264850.
[19] Loga T, Stein B, Diefenbach N. TABULA building typologies in 20 European countries—Making energy-related features of residential building stocks comparable. Energy and Buildings 2016;132:4–12. https://doi.org/10.1016/j.enbuild.2016.06.094.
[20] Jordan U, Vajen K, Kassel U. DHWcalc: PROGRAM TO GENERATE DOMESTIC HOT WATER PROFILES WITH STATISTICAL MEANS FOR USER DEFINED CONDITIONS n.d.:6.
[21] Braas H, Jordan U, Best I, Orozaliev J, Vajen K. District heating load profiles for domestic hot water preparation with realistic simultaneity using DHWcalc and TRNSYS. Energy 2020;201:117552. https://doi.org/10.1016/j.energy.2020.117552.
[22] Ayele GT, Haurant P, Laumert B, Lacarrière B. An extended energy hub approach for load flow analysis of highly coupled district energy networks: Illustration with electricity and heating. Applied Energy 2018;212:850–67. https://doi.org/10.1016/j.apenergy.2017.12.090.
[23] Huang W, Zhang N, Wang Y, Capuder T, Kuzle I, Kang C. Matrix modeling of energy hub with variable energy efficiencies. International Journal of Electrical Power & Energy Systems 2020;119:105876. https://doi.org/10.1016/j.ijepes.2020.105876.
[24] IBM® Decision Optimization CPLEX® Modeling for Python n.d. http://ibmdecisionoptimization.github.io/docplex-doc/index.html (accessed May 13, 2020).
[25] Persson U, Wiechers E, Möller B, Werner S. Heat Roadmap Europe: Heat distribution costs. Energy 2019;176:604–22. https://doi.org/10.1016/j.energy.2019.03.189.
[26] Energie Plus. Chaudières à condensation [chauffage]. Energie Plus Le Site n.d. https://energieplus-lesite.be/techniques/chauffage10/chauffage-a-eau-chaude/chaudieres-a-condensation/.
[27] Generation of electricity and district heating. Danish Energy Agency; 2020.
[28] JENSEN J. K, OMMEN T, REINHOLDT L, Et Al. Heat pump COP, part 2: generalized COP estimation of heat pump processes. 2018. https://doi.org/10.18462/IIR.GL.2018.1386.
[29] Boudéhenn F, Bonnot S, Demasles H, Lefrançois F, Perier-Muzet M, Triché D. Development and Performances Overview of Ammonia-water Absorption Chillers with Cooling Capacities from 5 to 100 kW. Energy Procedia 2016;91:707–16. https://doi.org/10.1016/j.egypro.2016.06.234.
[30] Ecoheatcool - The European Cold Market - Final Report. Euroheat&Power; 2005.
[31] Photovoltaic Geographical Information System 2022. https://re.jrc.ec.europa.eu/pvg_tools/fr/tools.html (accessed June 5, 2020).
[32] Reda I, Andreas A. Solar position algorithm for solar radiation applications. Solar Energy 2004;76:577–89. https://doi.org/10.1016/j.solener.2003.12.003.
[33] EU Buildings Factsheets. Energy - European Commission 2017. https://ec.europa.eu/energy/eu-buildings-factsheets_en (accessed April 15, 2022).
[34] Buffa S, Cozzini M, D'Antoni M, Baratieri M, Fedrizzi R. 5th generation district heating and cooling systems: A review of existing cases in Europe. Renewable and Sustainable Energy Reviews 2019;104:504–22. https://doi.org/10.1016/j.rser.2018.12.059.
[35] Fleiter T, Manz P, Neuwirth M, Mildner F, Persson U, Kermeli K, et al. Documentation on excess heat potentials of industrial sites including open data file with selected potentials 2020. https://doi.org/10.5281/zenodo.3896381.
[36] Eurostat n.d. https://ec.europa.eu/eurostat/en/data/database (accessed December 1, 2020).
[37] Heat Roadmap Europe. Biomass prices (D6.1 Appendix 2) 2017.
[38] ADEME. Centre de ressources sur les bilans de gaz à effet de serre. Site Bilans GES 2020. https://www.bilans-ges.ademe.fr/ (accessed May 25, 2020).

[39] Transparency Platform restful API - User guide n.d. https://transparency.entsoe.eu/content/static_content/Static%20content/web%20api/Guide.html (accessed February 22, 2021).
[40] Heating installations. Danish Energy Agency; 2018.
[41] Energy transport. Danish Energy Agency; 2020.
[42] Energy storage. Danish Energy Agency; 2020.
[43] Kusuda T, Achenbach PR. Earth temperature and thermal diffusivity at selected stations in the United States 1965:236.
[44] Huld T, Müller R, Gambardella A. A new solar radiation database for estimating PV performance in Europe and Africa. Solar Energy 2012;86:1803–15. https://doi.org/10.1016/j.solener.2012.03.006.
[45] Solar Keymark n.d. http://www.solarkeymark.nl/DBF/ (accessed April 4, 2022).